Automatic grid construction for few-body quantum mechanical calculations

V. Roudnev, Michael Cavagnero

Department of Physics and Astronomy, University of Kentucky, 600 Rose Street, Lexington, KY, 40506, USA

Abstract

An algorithm for generating optimal nonuniform grids for solving the two-body Schrödinger equation is developed and implemented. The shape of the grid is optimized to accurately reproduce the low-energy part of the spectrum of the Schrödinger operator. Grids constructed this way are applicable to more complex few-body systems where the number of grid points is a critical limitation to numerical accuracy. The utility of the grid generation for improving few-body calculations is illustrated through an application to bound states of He trimers.

Keywords: Quantum few-body calculations, Nonuniform grids, Optimization, Grading function, Faddeev equations

Introduction

The dynamics of few-body systems remains a robust field of research with many practical applications. A number of theoretical advances, coupled with increased computational resources, have lead to significant advances in both

---

the understanding of few-body processes and in the number of physical systems that can be successfully treated with existing, well-tested methodologies (see [2, 3, 4, 5, 6, 7, 8, 9] and references therein). We are, for example, currently developing public source code and a graphical user interface for scientists interested in solving Faddeev equations numerically for a wide array of potential three-body applications. Challenging computations that have been accessible to only a small group of specialists will soon become elementary and well characterized tools used by a large number of practitioners in different fields.

Solving the two-body Schrödinger equation numerically is an elementary exercise in the case of smooth central potentials. Typically, the power of modern computers makes it possible to use even the simplest numerical approaches to perform quite accurate calculations of the low-energy part of the two-body spectrum. Three-or-more-body calculations, however, usually require greater attention to the details of numerical technique, as the required computer resources usually scale geometrically with the growth of dimensionality of the problem, and optimizing any aspect of the solution representation leads to substantial computational savings.

When solving bound state or scattering problems for few-body systems it is important to treat the states of two-body subsystems carefully, as such states represent the asymptotic boundary conditions for the corresponding few-body states. It is also important to minimize the computational cost of reproducing every asymptote of the few-body calculations. The key feature of the Faddeev approach to few-body problem is the asymptotic factorability of the solutions, so that grids constructed for the efficient solution of the

two-body problem can be immediately employed with considerable numerical advantage. In previous calculations [11, 12, 13] this optimization has been performed manually. The procedure, however, is very time consuming and difficult for an inexperienced user or a student. Therefore, we needed an automatic procedure of constructing an effective grid representation of the two-body subsystems.

Methods of refining grids automatically are often used in solving various nonlinear evolution equations (hydrodynamical equations, for example) to reproduce discontinuities and other singular features of the solutions. In contrast,our goal is to create a software package specifically designed to solve the quantum-mechanical few-body problem, fully exploiting the features intrinsic to the physical problem and the numerical techniques to achieve high-performance of the resulting code. We therefore needed a solution which is on the one hand more specific to our problem, and on the other hand allows us to construct the grids on the base of some clearly understood physical and mathematical principles, with particular emphasis on reproducing the low-energy part of the two-body Schrödinger operator for subsequent use in more complex few-body calculations.

In this paper we describe and implement a practical nonuniform grid suitable for reproducing the low-energy part of the Schrödinger operator for two-body systems. When applied to systems of more than two particles, this grid permits a several-fold reduction in the number of grid points required for a desired level of numerical accuracy. Equally important, the procedure of constructing the grid is automatic and requires only minimal interference from a user.

1. Basic principles

We are solving the Schrödinger equation for a two-body system with central potentials using $S_{3,2}$ or $S_{5,3}$ Hermite splines and collocations at Gaussian points. We are constructing a nonuniform grid from the requirement of uniformity of the numerical error over the entire range where the solution is constructed.

Let us start from the radial Schrödinger equation in atomic units (a.u.) chosen so that $\hbar = e = m_e = 1$

$$(-\frac{1}{2\mu}\frac{d^2}{dx^2} + \frac{l(l+1)}{x^2} + V(x) - E_i)\varphi(x; \epsilon_i) = 0 \tag{1}$$

where μ is the reduced mass of the two-body system, subject to the Dirichlet boundary conditions

$$\varphi(0) = \varphi(x_{max}) = 0 \quad . \tag{2}$$

The right boundary of the interval x_{max} is assumed to be chosen so that its influence can be neglected. Let $\Delta_{N,\chi} \equiv \{0, x_1, \ldots, x_N\}$ be a grid constructed over the interval $[0, x_N = x_{max}]$ consisting of N intervals, χ is the map used to construct the nonuniform grid from a uniform grid. Particularly, $x_i = x_{max}\chi(i/N)$. The map $\chi : [0, 1] \to [0, 1]$ is a smooth function growing monotonically over the interval $[0, 1]$.

The criterion we choose for constructing χ is the uniformity of numerical error over the whole interval $[0, x_{max}]$. An approximate solution constructed with N points deviates from the exact solution by

$$\varphi^{(N)}(x) = \varphi(x) + \text{residue}_N(x)$$

At each sub-interval $[x_i, x_{i+1}]$ the residue norm can be estimated as

$$||\text{residue}_N(x)|| \le C_i(x)|x_{i+1} - x_i|^{k+1} + o(|x_{i+1} - x_i|^{k+1})$$

4

where $x \in [x_i, x_{i+1}]$ and k is the order of the spline [10]. The factors $C_i(x)$ are determined by the properties of the equation and the chosen numerical scheme. We can optimize the distribution of the grid points so that the error $||C_i(x)|x_{i+1} - x_i|^{k+1}||$ has the same order of magnitude throughout the whole interval. It is useful to treat the length $h_i = |x_i - x_{i-1}|$ of the i-th interval as a continuous function $h(u)$. The function $h(u)$ is naturally related to the derivative of the map $\chi(u)$

$$h_i = (x_i - x_{i-1}) = x_{max}(\chi(\frac{i}{N}) - \chi(\frac{i-1}{N})) = \frac{x_{max}}{N}\chi'(\frac{i-1/2}{N}) + O(\frac{1}{N^2}) \quad (3)$$

and

$$h_i = h(\frac{i-1/2}{N}) + O(\frac{1}{N^2}) \quad .$$

So, for sufficiently dense grids the i-th grid step is determined by the slope of the mapping function.

If $\epsilon(t)$ is some non-negative function, termed the "grading function", that characterizes the local approximation error, then the integral

$$\chi^{-1}(u) = \frac{\int_0^{ux_{max}} \epsilon(x)dx}{\int_0^{x_{max}} \epsilon(x)dx} \quad , \quad (4)$$

provides a monotonic map connecting the non-uniform grid with a uniform one. $\chi(u)$ is referred to herein as the "mapping function". If the grading function is chosen so that it peaks in the regions that are the most difficult to reproduce numerically, the inverse of the mapping function $\chi^{-1}(u)$ will grow the most rapidly in the corresponding regions. The mapping function, therefore, will have smaller derivative. It will make the nonuniform grid denser where the function is more difficult to reproduce. Characterizing the difficulty of representing the object function, the grading function can be

5

linked to some derivative of the function being interpolated. For example, if using a linear interpolant, the error of approximation will be of the order of the second derivative of the interpolated function. A quantitative characterization of the error and optimal properties of the grading functions have been studied in Ref. [1]. We shall use the approach of Ref. [1] for constructing an optimal map for solving Eq. 1.

Suppose we have a sample function $\varphi(x)$ for which we seek a piece-wise polynomial approximant $\tilde{\varphi}(x)$. It is shown in Ref. [1] that in order to minimize the L_2-norm of the error function $\| \varphi - \tilde{\varphi} \|_{L_2}$ the grading function $\epsilon(t)$ should be chosen as

$$\epsilon(x) = |\frac{d^{k+1}}{dx^{k+1}}\varphi(x)|^{\frac{2}{2k+3}} \quad ,$$

where k is the order of the polynomial approximant. According to [1] this grading function provides an asymptotically L_2-optimal grid for a sufficiently large N, when the $O(N^{-2})$ term in the equation (3) can be neglected.

There are a few complications with implementing this approach directly. The exact sample function $\varphi(x)$ is unknown. Moreover, our goal is an accurate approximation of an invariant subspace of the two-body Hamiltonian which is characterized by several functions that are the eigenvectors of the Hamiltonian. Those complications, however, are not critical.

If we redefine the norm to be optimized for a vector function composed of a set of eigenfunctions of the Hamiltonian $\{\varphi_1(x), \varphi_2(x), \ldots, \varphi_n(x)\}$, the optimal grading function takes the form

$$\epsilon(x) = (\sum_{m=1}^{n} |\frac{d^{k+1}}{dx^{k+1}}\varphi_m(x)|^2)^{\frac{1}{2k+3}} \quad . \tag{5}$$

Although the explicit form of the functions $\varphi_m(x)$ is generally unknown, for

our purpose we can use numerical approximation of these functions obtained on non-optimal grids. The resulting suboptimal estimates can be refined iteratively.

In the following sections we shall provide a few examples of how this approach can be realized in practice.

2. Implementation

Before describing the grid construction algorithm itself, we shall briefly outline the discretization procedure for the simplest case of zero angular momentum $l = 0$. For discretization we use the orthogonal collocation scheme [10] with the $S_{5,3}$ splines [11]. We shall seek for a solution of Eq. (1) an expansion in terms of B-spline basis in the spline space $S_{5,3}(\Delta)$ constructed for a given mesh Δ

$$\varphi_m(x) \approx \sum_{j=1}^{M} f_{m,j} B_j(x) \quad .$$

Functions $B_j(x)$ are constructed to satisfy the appropriate boundary conditions. Requiring the equation (1) to be satisfied exactly in the given set of collocation points x_k, $k = 1, 2, \ldots, M$ we reduce the equation to the (generalized) eigenvalue problem

$$(-\hat{D}_2 + \hat{V} - E_m \hat{B}) f_m = 0 \quad .$$

Here $\hat{D}_2$, $\hat{V}$ and $\hat{B}$ are square matrices

$$[\hat{D}_2]_{ij} = \frac{1}{2\mu} B_j''(x_i) \quad ,$$

$$[\hat{V}]_{ij} = (V(x_i) + \frac{l(l+1)}{x_i^2}) B_j(x_i) \quad ,$$

$$[\hat{B}]_{ij} = B_j(x_i) \quad .$$

The number of collocation points M – and the number of elements of the basis $B_j(x)$ – depend on the chosen spline space and the number of grid points N. For $S_{3,2}$ splines and Dirichlet boundary conditions $M = 2N$. In the case of $S_{5,3}$ splines $M = 3N + 1$.

Following the strategy we described in the previous section, first we discretize the two-body Hamiltonian using some non-optimal grid Δ_0. A cubic mapping $\chi_0(u) = u^3$ is, usually, a good starting point.

Next, we construct a sequence of grids $\Delta_i = \Delta_{\chi_i,N}$ and the corresponding approximations to the lowest n eigenfunction $\varphi_{m,(i)}(x)$. Each subsequent grid Δ_{i+1} is constructed using equations (4) and (5) with approximate functions $\varphi_m(x) \equiv \varphi_{m,(i)}(x)$ obtained at the previous step. We repeat the process several times until the grading function is stabilized.

Straightforward implementation of this approach, however, may look unrealistic. Indeed, we seek a solution in terms of piecewise polynomial functions of 5-th order. Evaluation of the grading function, however, requires evaluation of the 6-th order derivative of the solution. We, therefore, can not differentiate the spline expansion of the solution directly. Instead, we apply the discrete analog of the second derivative operator $\hat{B}^{-1}\hat{D}_2$ three times. Each application projects the corresponding derivative function back into the spline basis and this way an approximate 6-th derivative of the solution can be obtained.

In Fig. 1 we show an example of the sequence of the grading functions and the corresponding mappings $\chi_i(u)$ for the LM2M2 (He-He) potential [14] and Ne-Ne potential (av5z+(3321) fit) [15] for $S_{3,2}$ splines (for $l = 0$ angular

momentum). In both cases we have chosen the number of states n in Eq. (5) as the number of bound states supported by the potential plus one, so that the grid is optimized to reproduce all the bound states plus the continuum state closest to the threshold that satisfies the boundary conditions (2). (The He-He potential supports one s-wave bound state and the Ne-Ne potential supports three.)

It takes only a few iterations for the grading function to converge. The grading function reaches its maximum in the potential well, rapidly falls at the repulsive core and slowly decays at larger distances. The inverse of the mapping function $\chi^{-1}(u)$, according to equation (4), rapidly grows at the values of u that correspond to the potential well, so that the mapping function $\chi(u)$ grows very slowly in a wide range of the parameter u. The grid steps, therefore, become much smaller in the important potential well region (see Eq. (3)).

In the next section we shall compare grids generated by the optimal mappings with other empirical choices.

3. Convergence of two-body bound states

How practical is the construction? Can we expect any computational savings in few-body calculations when using the optimal mappings compared to widely used simple power or exponential mappings? To answer this question let us study the convergence of the bound state energies for the two-body problem with respect to the number of grid points.

To study the convergence properties of the numerical procedure it is natural to represent the property of interest – the bound state energy for example
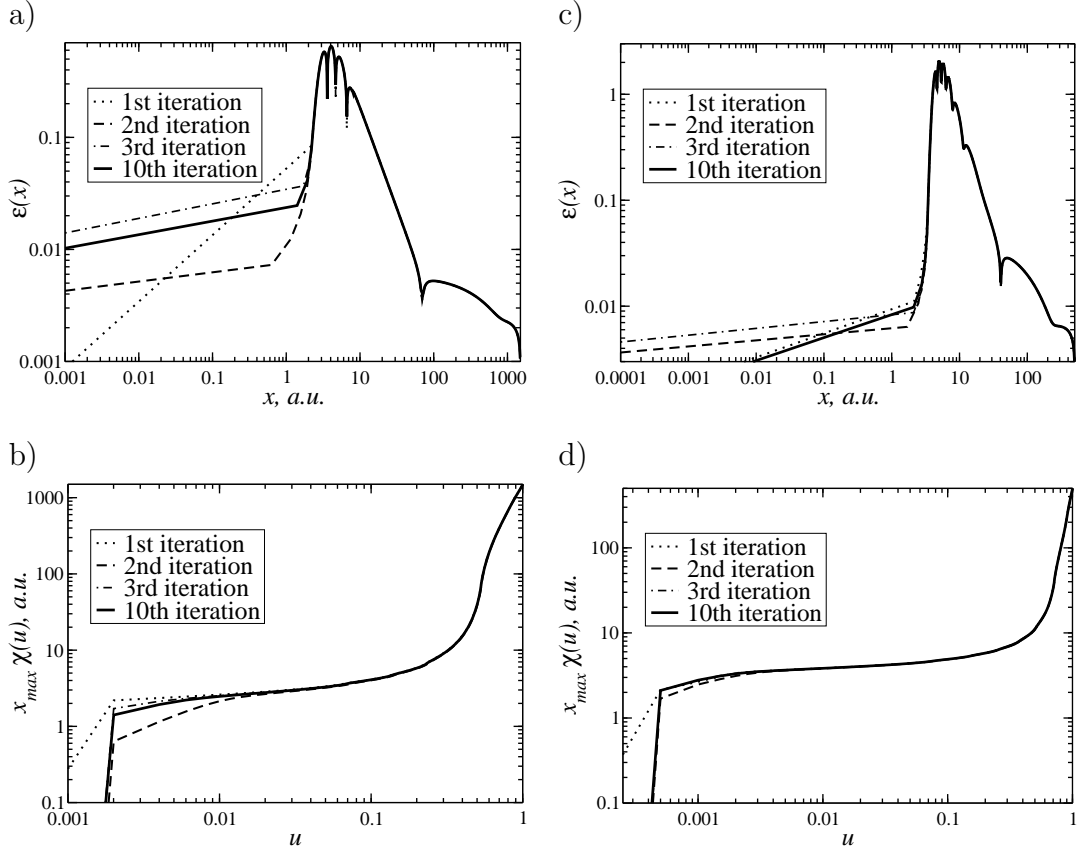
9

Figure 1: Grading functions and the corresponding mappings for He-He (left, a) and b)) and Ne-Ne potentials (right, c) and d)). The grading functions are maximal in the integration region $\sim 1 - 10$ a.u., as a result, the corresponding mapping functions have smaller derivatives ensuring smaller grid steps in the region of interaction.

– as a sum of two terms: the exact value and the grid-dependent numerical error

$$\tilde{E}^{(N)} = E + E_{err}(\Delta_{N,\chi}) \quad .$$

The numerical error depends on the number of grid points N, their distribution defined by the mapping χ and the boundary conditions. Here we shall assume that the boundary conditions are chosen so that they essentially do not contribute to the error, or can be taken into account analytically. We shall consider the following grid shapes

$$\begin{aligned}
\chi_{power}^n &= u^n \quad , \\
\chi_{exp}^n &= \frac{e^{nu}-1}{e^n-1}
\end{aligned}$$

for comparison with χ_{opt} defined by Eq. (4) and (5). To make this comparison we want to introduce a quantity which describes the character of convergence qualitatively.

The collocation methods used in this work are expected to converge with the rate $O(N^{-(k+1)})$ where k is the order of the spline. It is, therefore, natural to parametrize the numerical error by the inverse number of grid points $\frac{1}{N}$. The error term $E_{err}(\frac{1}{N})$ does not behave regularly with the number of grid points and it is difficult to estimate it exactly. Its absolute value, however, should behave as $\frac{1}{N^{k+1}}$. To characterize the convergence obtained with a particular mapping χ we shall fit the numerical values obtained with the given number of points $\tilde{E}_N$ as

$$\tilde{E}^{(N)} = E + C\frac{1}{N^{k+1}} \quad . \tag{6}$$

The coefficient C characterizes the speed of convergence and E gives a more accurate estimate for the energy of the bound state. Both the speed of

11

convergence C and the extrapolated energy estimate E discussed below are obtained by least square fits of the expression (6) to data sets similar to the one shown in Fig. 2. When fitting we gave bigger weights to the values obtained with denser grids. Having a finite number of points in each data set, we can extract estimates for E and C only with finite accuracy. As we have mentioned above, the error term does not behave monotonically, which makes it difficult to obtain very accurate estimates of E and C. [1] For the extrapolated energy estimate E we make sure that the error of the estimated value is comparable with systematic errors of different origins, such as the error introduced by an approximate boundary condition at the right end of the interval.

To illustrate the meaning of the coefficient C, in Fig. 2 we show the convergence plots for the bound state energy of He_2 calculated with three different mappings: χ_{opt}, χ_{exp}^8 and χ_{power}^4. In Fig 2a) the fit of the bound state energy convergence for $S_{3,2}$ splines is shown. The method of orthogonal collocations that we employ is not variational, and the error for the Hamiltonian eigenvalues is expected to have the same order of accuracy as the wave function. The computational error, therefore, should scale as $O(N^{-4})$. We

---

[1]We see two sources of this non-monotonic behavior. First, the collocation scheme that we employ does not give an optimal variational estimate for the energy, therefore, when the grid is sparse, the deviation of the energy estimate from an optimal value is comparable with the error of approximation of the wave function. There is also a second source of non-monotonic behavior which influences even variational estimates of the energy and becomes evident for very dense grids: when increasing the number of grid points the spline space itself does not approach the invariant subspace of the Hamiltonian monotonically. This second effect, however, is much smaller than the first one.
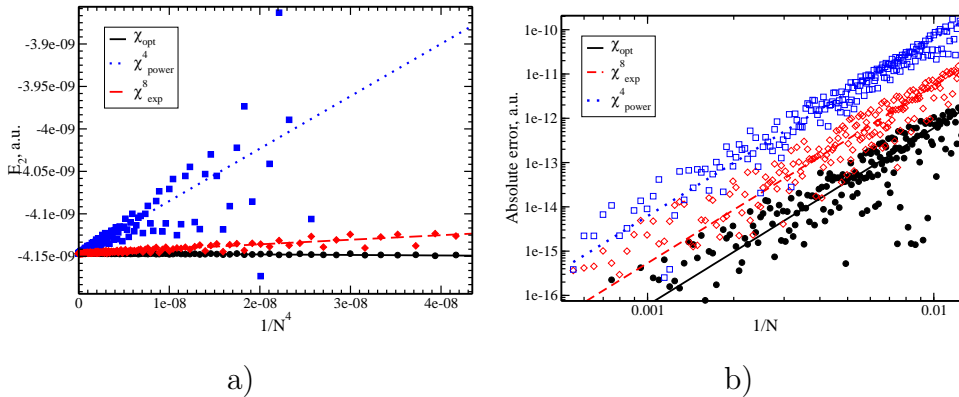
Figure 2: Convergence of the He$_2$ bound state energy for LM2M2 potential

do observe this kind of scaling in Fig. 2a-b. The speed of convergence coefficient C corresponds to the slope of the lines in Fig. 2. It is important to note that as the coefficient C is calculated from the fits, its typical relative error is of the order of 50%, its estimate may vary depending on a particular grid sampling used in the fitting procedure. We thus will report only one significant figure in the estimates of the coefficient C, and deviations of the coefficient estimate within the same order of magnitude can be considered insignificant. Accordingly, C gives the desired *qualitative measure* of a grid quality.

In Table 1 we report the fitted values of the speed of convergence coefficient. It is evident, that the error estimate for the optimal mapping is at least an order of magnitude smaller than for other considered grid choices. The result is not surprising, as can be seen from Fig. 3. Indeed, as the optimal mapping is not linear in logarithmic scale, simple power grids χ_{power}^m are not expected to produce a good approximation of the solution. The exponential mappings, on the other hand, can fit the optimal mapping more closely at
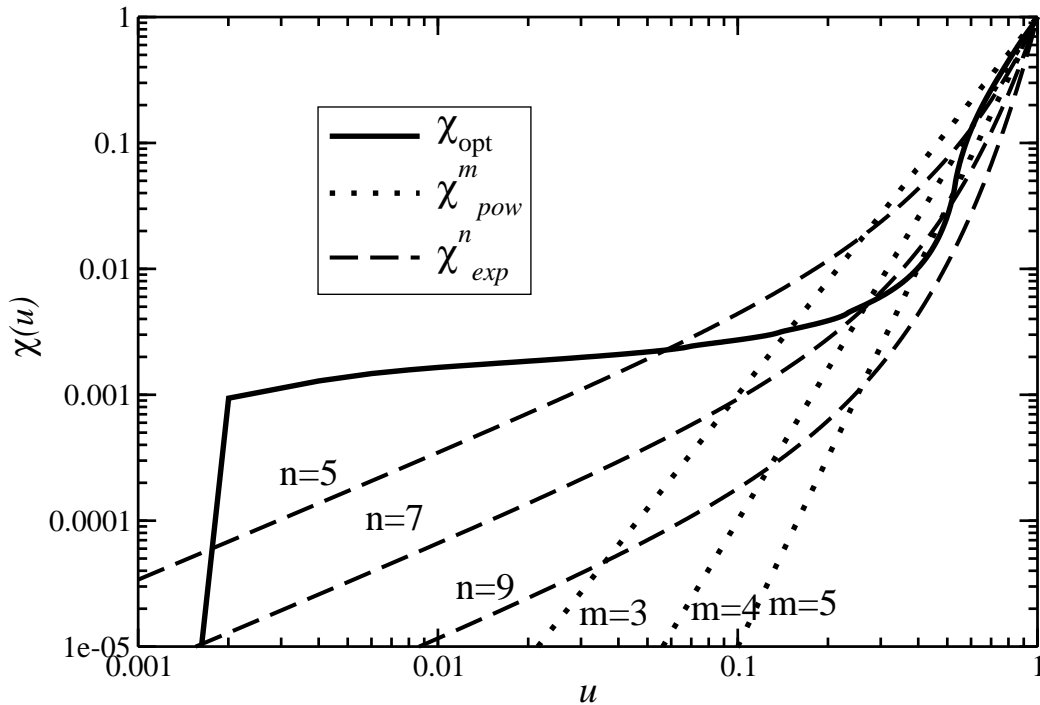
Figure 3: Optimal and suboptimal mappings for He_2.

$n \approx 8$, and the estimates of the speed of convergence for $n = 8$ are minimal within the set of exponential grids.

All the grids we demonstrated have been constructed for two-body states with zero orbital angular momentum $l = 0$ (Eq.1). When constructing grids for actual use in few-body calculations the bound states with higher angular momenta should also be reproduced accurately. The centrifugal barrier for these states is usually a small perturbation compared to the two-body force, so that at least for a few lowest angular momentum states explicit inclusion of the rotationally excited states into the grading function may be unnecessary. Let us compare the spectra of rotationally excited Ne_2 dimer obtained with the grid optimized for the s-wave with the spectra calculated with grids

He$_2$			
n	χ^n_{power}	χ^n_{exp}	χ_{opt}
3	1×10^{-2}	-3×10^{-1}	
4	6×10^{-3}	4×10^{-2}	
5	5×10^{-3}	5×10^{-3}	6×10^{-5}
6	5×10^{-3}	10^{-3}	
7	5×10^{-3}	6×10^{-4}	
8	6×10^{-3}	5×10^{-4}	

Ne$_2$			
n	χ^n_{power}	χ^n_{exp}	χ_{opt}
3	6	10^1	
4	3	3	
5	4	8×10^{-1}	-2×10^{-3}
6	6	6×10^{-1}	
7	7	7×10^{-1}	
8	7	1	

Ne$_2^*$			
n	χ^n_{power}	χ^n_{exp}	χ_{opt}
3	6	10^1	
4	3	2	
5	4	9×10^{-1}	-2×10^{-3}
6	6	7×10^{-1}	
7	2	8×10^{-1}	
8	7	1	

Ne$_2^{**}$			
n	χ^n_{power}	χ^n_{exp}	χ_{opt}
3	2×10^{-1}	3×10^{-1}	
4	1×10^{-1}	8×10^{-2}	
5	1×10^{-1}	3×10^{-2}	-3×10^{-6}
6	2×10^{-1}	2×10^{-2}	
7	3×10^{-1}	3×10^{-2}	
8	2×10^{-1}	4×10^{-2}	

Table 1: Estimates of the convergence speed C for the He_2 and Ne_2 s-wave bound state energies for different grid shapes

	Ground				1st excited				2nd excited
l_{opt}	1s	1p	1d	1f	2s	2p	2d	2f	3s
0	-2e-3	-2e-3	-2e-3	-2e-3	-3e-3	-3e-3	-2e-3	-2-e3	-2e-6
1	-2e-3	-2e-3	-2e-3	-2e-3	-3e-3	-3e-3	-2e-3	-3e-3	1e-3
2	-3e-3	-3e-3	-3e-3	-3e-3	-4e-3	-4e-3	-4e-3	-3e-3	5e-4
3	-4e-3	-4e-3	-3e-3	-3e-3	-5e-3	-5e-3	-4e-3	-4e-3	5e-4

Table 2: Ne_2 speed of convergence of the rotationally excited states. The optimal mapping χ_{opt} has been constructed for the states with angular momentum quantum number l_{opt}, the corresponding speed of convergence coefficients C for the energies of the low-lying bound states are shown.

optimized for a given angular momentum. We report the estimates for the speed of convergence for s-, p-, d- and f-waves in Table 2.

We have optimized the grid to reproduce 5 lowest eigenstates of the two-body Hamiltonian with angular momentum l_{opt} and used those grids to calculate the ground state and low-lying vibrationally and rotationally excited states of the system. The extrapolated energy estimates (see the discussion for Eq. 6) agree excellently at the level of 10^{-13} a.u., which is comparable with the error introduced by the cut-off distance of 500 a.u. As expected, optimizing the grid for the s-wave spectrum provides a very good basis for reproducing the rotationally excited states. Optimizing the grid for the rotationally excited states similarly gives very good results for the lowest two s-wave vibrational states. The convergence for the near-threshold s-wave state, however, is getting much slower, although still comparable with the speed of convergence for the low-lying states. We therefore conclude that only the s-wave optimization is needed to provide a good description of processes

involving the few lowest rotational excitations.

The other important question is how many states should be included in the grading function (5). From Table 3 we can conclude that the very minimal number of states to be included in the grading function to reproduce the discrete spectrum of the operator should be equal to the number of the s-wave bound states. When including more states into the grading function the convergence of the bound state energies is getting insignificantly slower. We can expect, however, that the states from the continuum start being reproduced better. To check the convergence of the continuum states we fit the low-energy expansion for the s-wave scattering phase

$$k \cot \delta_0(k) = -\frac{1}{a} + \frac{r_0 k^2}{2} + X k^4 + O(k^6) \tag{7}$$

to the spectrum of the discretized Hamiltonian[2] and calculate the convergence coefficients of the effective range parameters, in quite the same manner as was done for the binding energy (Table 4). To estimate the scattering parameters we used the six lowest positive eigenvalues of the Hamiltonian. As there are three bound states in the system, it is not surprising that the fastest convergence is obtained with nine states included in the grading function. Similar to the bound state case, including extra states into the grading

---

[2] Note that the energies of the discretized continuum are determined by the scattering phase and the boundary condition at the right end R of the interval. For the s-wave states the wave function behaves as $\sin(kR+\delta(k))$, and the phase shifts can be recovered from the positive energy spectrum E_n and the box size R using the condition $\sqrt{E_n}R + \delta(\sqrt{E_n}) = \pi n$. For large R the number of energies E_n that fall in the region where the effective range expansion is valid becomes sufficient to extract the parameters of the effective range expansion.

	Ground				1st excited				2nd excited
n	1s	1p	1d	1f	2s	2p	2d	2f	3s
1	-1e-3	-1e-3	-1e-3	-1e-3	-3e-3	-3e-3	-4e-3	-6e-3	2e-1
2	-4e-4	-4e-4	-4e-4	-3e-4	-5e-4	-5e-4	-5e-4	-4e-4	-3e-2
3	-1e-3	-1e-3	-1e-3	1e-3	-2e-3	-2e-3	-1e-3	-1e-3	-2e-6
4	-1e-3	-1e-3	-1e-3	-1e-3	-2e-3	-2e-3	-2e-3	-2e-3	-2e-6
5	-2e-3	-2e-3	-2e-3	-2e-3	-3e-3	-3e-3	-2e-3	-2-e3	-2e-6
6	-3e-3	-3e-3	-2e-3	-2e-3	-4e-3	-4e-3	-3e-3	-3e-3	1e-7
7	-4e-3	-4e-3	-3e-3	-3e-3	-6e-3	-5e-3	-5e-3	-4e-3	4e-6
8	-5e-3	-5e-3	-4e-3	-4e-3	-8e-3	-7e-3	-7e-7	-6e-3	4e-6
9	-6e-3	-6e-3	-6e-3	-5e-3	-1e-2	-1e-2	-9e-3	-7e-3	1e-5
10	-8e-3	-8e-3	-7e-3	-6e-3	-1e-3	-1e-2	-1e-2	-1e-2	1e-5

Table 3: Ne$_2$: speed of convergence for the s-wave vibrational bound states and first 3 rotational excitations as a function of the number of optimized states.

function does not have much effect on the speed of convergence after all the states used for estimating the effective range parameters have already been included.

Before discussing the application to three-body calculations, we provide a check of the suitability of the grading function suggested in Ref. [1]. For this purpose we compare the speed of convergence obtained with different values of k in Eq. 5, but holding the order of the polynomial k' fixed, and check whether the value of $k = k'$ provides the best speed of convergence. We summarize our observations in Tables 5, 6 and 7. In Table 5 we summarize our convergence speed analysis for the He$_2$ dimer bound state energy (LM2M2

n	C(a), a.u.	C(r0), a.u.	C(X), a.u.^{3}
2	6e12*	4e10*	5e13*
3	3e8	-6e9	6e12*
4	4e5	-7e6	6e9
5	4e5	-5e6	4e9
6	2e4	-5e5	6e8
7	7e4	-8e5	5e8
8	-2e4	3e5	-2e8
9	1e4	2e4	6e7
10	2e4	-4e4	8e7
11	3e4	-4e4	7e7
12	3e4	-4e4	6e7

Table 4: Ne-Ne scattering parameters speed of convergence as a function of the number of states included in the grading function. Those data points marked with an asterisk indicate a failed convergence estimate.

potential [14]) with the grid optimized for the ground and one continuum state. The theoretically optimal values are shown in bold font. In Table 6 we show the same data for the grids optimized for the bound state only. The lower values of k correspond to bigger variations of the mesh points density distributions, the bigger the k the more uniform the grid is. We can easily observe that for the values of k considerably different from the optimal values the speed of convergence essentially deteriorates. For the values of k a little bit smaller than the theoretically optimal one, however, the observed speed of convergence can be close to the optimal or even demonstrate a little better convergence. In the case of two states included into the grading function (Table 5) this can be partially attributed to the fact that the grading function is actually optimized for more than one state which we are tracking. However, we observe similar behavior even if we optimize the grid to reproduce the bound state only. As our grids are constructed on the base of an iterative numerical procedure which is not proved to be exact and the speed of convergence parameter is intended as a qualitative measure of the convergence properties, this minor deviation of the observed optimal k from the theoretically optimal value can not be considered evident (see the discussion for Eq. (6)). It is also useful to note that when the value of k exceeds the theoretically optimal value, the coefficient C starts to grow rapidly.

In Table 7 we report the speeds of convergence for the energies of the s-wave bound states of the Ne_2 dimer. We have optimized the grid to reproduce the three bound states of the dimer and one state from the continuum. The speed of convergence coefficient for the near-threshold state clearly reaches its minimum at the theoretically optimal value of k, which confirms the

	$S_{3,2}$		$S_{5,3}$	
k	E_2(extrapolated)	C	E_2(extrapolated)	C
6	-4.146595e-09	2e-4	n/a	n/a
7	-4.146597e-09	2e-5	n/a	n/a
8	-4.146598e-09	-1e-5	n/a	n/a
9	**-4.146596e-09**	**-5e-5**	-4.146638e-09	-2e-2
10	-4.146598e-09	-1e-4	-4.146578e-09	3e-4
11	-4.146598e-09	-3e-4	-4.146577e-09	8e-4
12	-4.146608e-09	-6e-4	-4.146579e-09	1e-4
13	-4.146636e-09	-1e-3	**-4.146581e-09**	**6e-4**
14	-4.146658e-09	-1e-3	-4.146573e-09	-5e-4
15	-4.146751e-09	-9e-4	-4.146586e-09	2e-3
16	-4.146510e-09	-1e-2	-4.146581e-09	-7e-3

Table 5: Optimality check of the automatically generated grids: He$_2$ bound state energy (a.u.) and the speed of convergence for different values of k in Eq. (5). The grading function is optimized for $n = 2$ states. Bold font indicates the asymptotically optimal choice [1].

	$S_{3,2}$		$S_{5,3}$	
k	E_2(extrapolated)	C	E_2(extrapolated)	C
6	-4.146595e-09	2e-4		
7	-4.146598e-09	2e-5		
8	-4.146595e-09	-1e-5		
9	**-4.146598e-09**	**-6e-5**	-4.146589e-9	-1e-2
10	-4.146597e-09	-2e-4	-4.146622e-9	8e-4
11	-4.146589e-09	-3e-4	-4.146634e-9	8e-4
12	-4.146625e-09	-7e-4	-4.146624e-9	4e-4
13	-4.146597e-09	-2e-3	**-4.146631e-9**	**4e-4**
14	-4.146551e-09	-2e-3	-4.146642e-9	-6e-4
15	-4.146658e-09	-2e-3	-4.146650e-9	2e-3
16	-4.146452e-09 -	-6e-3	-4.146649e-9	-3e-3
17	-4.146679e-09	-1e-2	-4.146655e-9	7e-3
18	-4.146670e-09	-1e-2	-4.146656e-9	-2e-2
19	-4.146366e-09	-6e-3	-4.146574e-9	-7e-2
20	-4.146584e-09	3e-2	-4.146598e-9	-3e-1

Table 6: Optimality check of the automatically generated grids: He$_2$ bound state energy (a.u.) and the speed of convergence for different values of k in Eq. (5). The grading function is optimized for the bound state only. Bold font indicates the asymptotically optimal choice [1].

	$S_{3,2}$			$S_{5,3}$		
k	C_{Ne_2}	$C_{Ne_2^*}$	$C_{Ne_2^{**}}$	C_{Ne_2}	$C_{Ne_2^*}$	$C_{Ne_2^{**}}$
6	-2e-5	-2e-5	3e-3	n/a	n/a	n/a
7	-2e-4	-5e-4	5e-4	n/a	n/a	n/a
8	-6e-4	-1e-3	1e-4	n/a	n/a	n/a
9	**-1e-3**	**-2e-3**	**4e-6**	-3e-2	8e-2	-2e-2
10	-2e-3	-3e-3	-5e-5	-3e-2	1e-2	1e-4
11	-4e-3	-5e-3	-8e-5	-9e-2	3e-3	2e-3
12	-3e-3	-5e-3	-3e-5	-2e-1	-6e-3	9e-4
13	2e-3	2e-3	2e-4	**-7e-1**	**-3e-2**	**-7e-4**
14	2e-2	2e-2	9e-4	-2	-9e-2	-4e-3
15	2e-2	2e-2	1e-3	-4	-2e-1	-1e-2
16	5e-3	4e-2	2e-3	-4	-4e-1	-2e-2

Table 7: Optimality check of the automatically generated grids: the speed of convergence for the Ne$_2$ dimer s-wave states. Bold font indicates the asymptotically optimal choice [1].

practicality of our approach.

4. The three-body calculations with optimized grids

As mentioned in the introduction, the practical value of optimizing the grids for two-body states lies in their application to more complex few-body calculations. In this case, reducing the number of points needed to achieve the required accuracy is critical for saving computational time. The direct use of the two-body optimized grids described in the previous section is especially appropriate in the Faddeev (three-body)[11, 12, 13] or Faddeev-Yakubovsky (four-body) [2, 9] formalism. When solving the Faddeev equations, as we shall briefly discuss below, it is natural to represent the grid as a direct product of the grid supporting the two-body bound states, and grids describing other coordinates in the configuration space of the three-body system. We shall demonstrate, that optimizing the grid even in one of the coordinates can improve the accuracy of the three-body calculations substantially.

Here, for simplicity, we shall discuss only the three-body calculations below the three-body threshold, which physically means that we restrict our attention to three-body bound states or scattering with only two clusters in the initial and the final states of the system. Within the Faddeev approach the wave function of such states resolves into a sum of three components

$$\Psi = \Phi_1(x_1, y_1) + \Phi_2(x_2, y_2) + \Phi_3(x_3, y_3)$$

that correspond to different partitionings of the three-body system into an interacting two-body subsystem and the free third particle. x_i and y_i are the Jacobi coordinates for the i-th partitioning: x_i connects the particles in the

24

$i - th$ pair, y_i points to the remaining particle from the i-th pair center of mass. The asymptotic properties of the components Φ_i below the three-body threshold are very simple: at large distances between the i-th particle and the center of mass of the corresponding two-body cluster ($|y_i| \to \infty$), the Faddeev components factorize. In the very simplest case of one single s-wave bound state in the pair the components Φ_i behave as

$$\Phi_i \sim \phi_2(|x_i|) f(|y_i|) \quad ,$$

where $\phi_2(|x_i|)$ is the wave function of the two-body subsystem and $f(|y_i|)$ describes the free motion of the third particle. When solving the Faddeev equation numerically, we, therefore, need to be able to reproduce the behavior of the two-body clusters accurately. For this purpose we use the grid optimization procedure described above. In principle, it is also possible to develop some simple criteria for optimizing grids in the reaction coordinates y. This problem, however, is beyond the goals of this paper and we shall discuss it elsewhere.

In order to demonstrate the importance of using optimized two-body grids in three-body calculations we have performed a series of calculations of He$_3$ ground and excited states with both optimized and non-optimized grids using a different number of points in the cluster coordinates. The number of points as well as the grid shape in the reaction coordinate y has been fixed for all sets of calculations. We used 100 grid points with $S_{5,3}$ splines in the y coordinate, the cutoff radius has been set to $y_{max} = 2000 \times \sqrt{3}/2$ a.u. and $\chi_{exp}^{(4)}$ mapping has been used to construct the non-uniform grid. As our three-body calculations here are only for purposes of demonstration, we used the simplest possible grid consisting of one single

interval in the angular coordinate (which is the cosine of the angle between the direction to the third particle and the axis of the He_2 cluster). We used $S_{5,3}$ splines in the angular coordinate. In this case the angular basis reduces to polynomials of 5-th degree. The angular symmetry of the system has not been taken into account explicitly, and, effectively, such angular basis corresponds to taking into account two first virtual rotational excitations ($l = 0, 2, 4$). More details on the method we use to solve Faddeev equations can be found in [11, 12, 13]. The results are shown in Figs. 4 and 5, where we have plotted the energies of the trimer bound states calculated using $S_{3,2}$ (Fig. 4) and $S_{5,3}$ splines (Fig. 5) as functions of the (appropriately scaled) number of grid points in the cluster coordinate. In both cases we observe much faster convergence and much smaller variation of the numerical results when using the optimized grids in cluster coordinates. We obtained the following estimates of the $^4He_3$ bound state energies. With cubic splines and 100 grid points in x we find $E_0 = -3.98756 \times 10^{-7}$ a.u $= -125.917$ mK for the ground state and $E_1 = -7.1984 \times 10^{-9}$ a.u. $= -2.2731$ mK for the excited state. With quintic splines and 70 grid points the corresponding results are $E_0 = -3.9877 \times 10^{-7}$ a.u $= -125.920$ mK for the ground state and $E_1 = -7.1978 \times 10^{-9}$ a.u. $= -2.2729$ mK. These results agree perfectly well with previously reported independent results using the same angular basis (but a different projection operator) $E_0 = -125.9$ mK and $E_1 = -2.28$ mK [3]. They also agree with previously reported results (for the same angular basis) of one of the authors [11] $E_0 = -125.81$ mK and $E_1 = -2.2677$ mK obtained with a similar method using less dense manually fine-tuned grids[3]

---

[3] A slightly different coupling constant employed in previous calculations [11] makes for
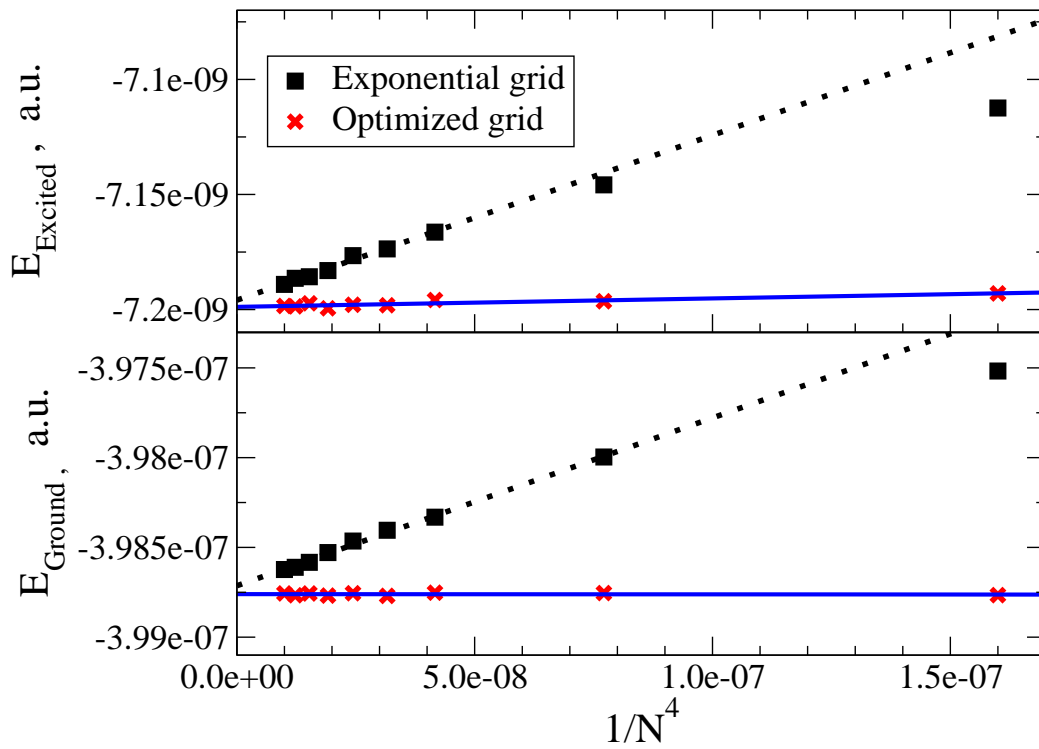
Figure 4: Energies of He$_3$ bound states calculated using $S_{3,2}$ splines as a function of the number of grid points in cluster coordinates
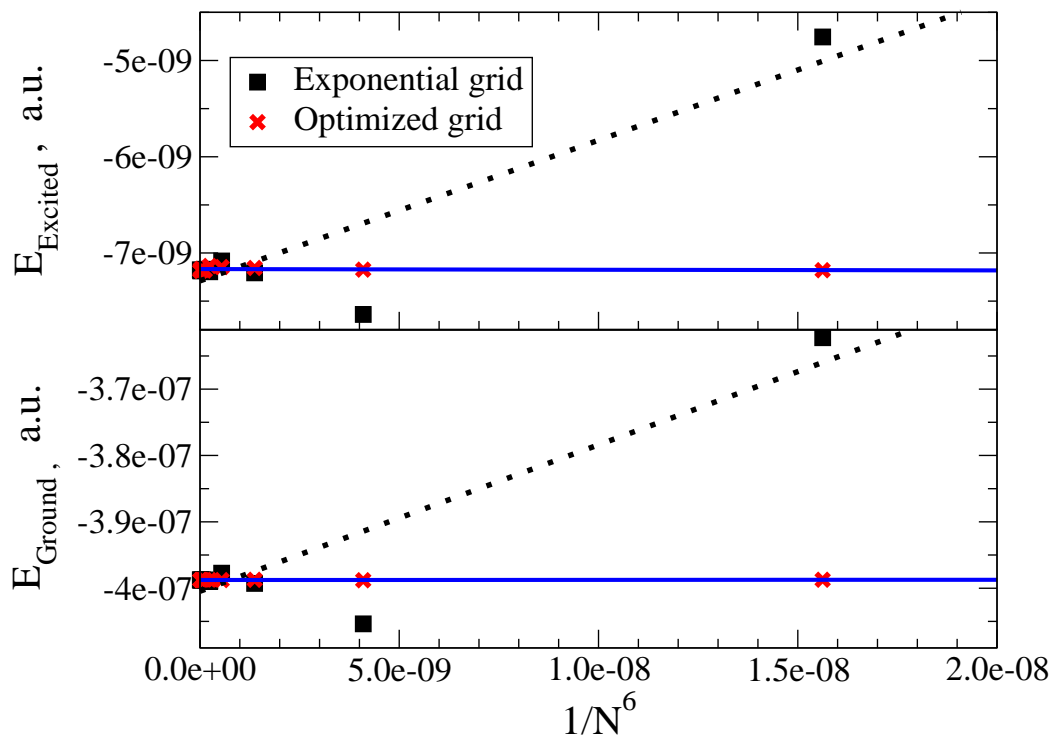
Figure 5: Energies of He_3 bound states calculated using $S_{3,2}$ splines as a function of the number of grid points in cluster coordinates.

5. Conclusions

We have presented an approach to constructing an optimized nonuniform grid for use in quantum few-body calculations. The approach is based on the results of Ref. [1], where a grading function which asymptotically minimizes the L_2 norm of the interpolation error is introduced. We have slightly modified the optimization criterion to have several low-lying eigenstates of the two-body Hamiltonian interpolated well.

We have studied the convergence properties of the optimized grids. For this purpose we have introduced the speed of convergence coefficient which characterizes the rate at which a physical observable – such as energy – converges as the number of grid points is increased. The optimized grids, even being only asymptotically optimal, demonstrate convergence properties superior to other choices of non-uniform grids routinely employed in few-body calculations. As far as rotational excitations of a two-body system can be taken into account perturbatively, it is sufficient to optimize the grids to reproduce the s-wave only and there is no need to optimize the grid for all the rotational excitations. The number of two-body states to be included into the grading function depends on the physical problem being solved. All the states that contribute to the long-range asymptote of the few-body system must be included into the grading function. Including some extra states can be beneficial, as it makes possible to account for the corresponding virtual

---

60% of the discrepancy for the excited state and 100% of the discrepancy for the ground state value. The sensitivity of the results to the details of the interaction is a subject of a separate study being prepared for publication.

excitations more accurately, while the convergence of the low-lying states is only slightly affected.

We have used the optimized grid in three-body calculations to describe cluster degrees of freedom. More accurate description of the internal dynamics of the colliding clusters leads to substantial improvements in the accuracy of calculations. The presented algorithm has allowed us to eliminate a difficult and time-consuming stage of manual fine-tuning the nonuniform grids to be used with a particular three-body system. This result is essential for the goals of our project to develop a simple and effective public code for low-energy quantum three-body calculations.

The presented algorithm has been constructed specifically for solving the quantum three-body problem with short-range interaction on the base of Faddeev equations. The approach itself, however, has an unexplored potential. Let us make a few remarks on other possible applications. Optimal grids for Coulomb systems can be considered. In this case the grading function can be constructed analytically. Adiabatic hypersphecical calculations can also benefit from adding a grid adaptation step after calculating the adiabatic basis for each value of the hyperradius. Finally, finding an effective method to optimize the "reaction" degrees of freedom in Faddeev calculations is a subject especially interesting for our project.

Acknowledgments

References

[1] Graham F. Carey and Hung T. Dinh, J. Numer. Anal. 22 (1985) 1028.

[2] A.K. Motovilov, Few Body Systems 43 (2008) 121.

[3] E. A. Kolganova, A. K. Motovilov and W. Sandhas, Physics of Particles and Nuclei 40 (2009) 206.

[4] D. Blume, Chris H. Greene and B.D. Esry, J. Chem. Phys. 113 (2000) 2145.

[5] Hiroia Suno and B.D. Esry, Phys. Rev. A 78 (2008) 062701.

[6] Hiroia Suno and B.D. Esry, Phys. Rev. A 82 (2010) 062521.

[7] P. Barletta and A. Kievski, Few-Body Systems 45 (2009) 123.

[8] H.Kamada *et al.*, Phys. Rev. C (2001) 044001.

[9] Rimantas Lazauskas and Jaume Carbonell, Phys Rev. A 73 (2006) 062717.

[10] C. de Boor and B. Swartz, SIAM J. Numer. Anal. 10 (1973) 582.

[11] V. A. Roudnev, S. L. Yakovlev, and S. A. Sofianos, Few-Body Systems 37 (2005) 179.

[12] V.A.Roudnev, Chem. Phys. Lett. 367 (2003) 95.

[13] V. Roudnev, Nucl. Phys. A 737CF (2003) S292.

[14] Ronald A. Aziz and Martin J. Slaman, J. Chem. Phys. 94 (1991) 8047.

[15] Sławomir M. Cybulski and Rafał R. Toczyłowski, J. Chem. Phys. 111 (1999) 10520.